THE ASTROPHYSICAL JOURNAL, 264:337–355, 1983 January 15

CCD PHOTOMETRY OF ABELL CLUSTERS. I. MAGNITUDES AND REDSHIFTS FOR 84 BRIGHTEST CLUSTER GALAXIES

DONALD P. SCHNEIDER
Palomar Observatory, California Institute of Technology
JAMES E. GUNN[1]
Princeton University
AND
JOHN G. HOESSEL
Kitt Peak National Observatory,[2] Space Telescope Science Institute[3]
Received 1982 May 21; accepted 1982 July 20

ABSTRACT

A sample of 84 Abell clusters has been selected to determine how the luminosity of the brightest cluster galaxy varies with cluster parameters. The clusters are of moderate redshift ($0.04 < z < 0.30$) and have a wide range of richness (Abell richness classes 0 to 5). Redshifts and two-color photometry for these galaxies are presented. A photometric system is developed which is well matched to the detector (low noise CCD) and to placing galaxies of vastly different redshifts on a standard system. These measurements are combined with earlier work to form a low redshift sample of 199 brightest cluster galaxies. The data confirm that the dispersion in the luminosities of first-rank cluster galaxies is ~ 0.34 mag. The colors of giant ellipticals have not changed since redshifts of 0.25. The trend of luminosity with Bautz-Morgan class matches those in previous investigations (~ 0.12 mag per class, with BM I being 0.3 mag brighter than the average cluster). The richness correction is reasonably well established at 0.10 magnitude per Abell richness class (rich clusters have brighter galaxies). There is a small uncertainty in the richness correction because the very rich clusters are, on average, more distant than the poorer ones. Application of these corrections reduces the luminosity dispersion slightly, to 0.29 mag.

Subject headings: cosmology — galaxies: clusters of — galaxies: photometry

I. INTRODUCTION

The redshift-magnitude relation, or Hubble diagram, is the classic test of the global properties of the universe. Several recent systematic studies (Gunn and Oke 1975 [GO]; Sandage, Kristian, and Westphal 1976 [SKW]; Kristian, Sandage, and Westphal 1978 [KSW]; Hoessel, Gunn, and Thuan 1980 [HGT]) have used the brightest cluster galaxy as a standard candle. The intrinsic dispersion in the aperture luminosity of these sources is ~ 0.35 mag, which is reduced to ~ 0.25 mag by applying corrections for morphological type, cluster richness, and galaxy structure (see KSW and HGT).

These investigations yielded values of q_0 from -0.55 to 1.7; the reason for this discrepancy is not yet understood, but probably arises in the selection and analysis procedures. Another major impediment to measuring a believable value for the deceleration parameter is the unfortunate fact that galaxies change as a result of the evolution of their stellar populations (Tinsley and Gunn 1976). The brightest cluster galaxies also experience significant changes because of their cannibalism of other cluster members induced by dynamical friction (Ostriker and Tremaine 1975; Gunn and Tinsley 1976; Hausman and Ostriker 1978; Hoessel 1980).

The measurements in HGT (116 galaxies) effectively determine the luminosity of first-ranked ellipticals at the present epoch. Since the HGT sample contains all high galactic latitude Abell clusters of richness greater than 0 and distance class less than 5 (except for $\delta < -25°$), it is impossible to substantially improve this data base. An investigation of a well-determined sample of clusters at high redshift (0.25–1.0) is described in Gunn, Hoessel, and Oke (1983). The present paper presents work on clusters of intermediate redshift ($z \sim 0.15$) with a wide range of properties including the very rich clusters which are missing in the nearby HGT sample.

The sample in this paper consists of 84 clusters chosen from Leir and van den Bergh's (1977, hereinafter

[1]Visiting Associate, Palomar Observatory.
[2]Operated by AURA, Inc., under contract with the National Science Foundation.
[3]Operated by AURA, Inc., on behalf of the National Aeronautics and Space Administration.

TABLE 1

DATA ON THE RICHNESS SAMPLE

Abell	R.A. 1950.0	Dec	l	b	R	D	BM	z	r	g-r	Gal Abs	G I	RAM
22	00 18 12	-25 59 20	42.9	-83.0	3	6	I	0.1432 *	16.44	+0.67	0.02	16.58	20.88
34	00 24 47	-09 04 57	104.5	-70.8	2	6	I-II	0.0410	15.47	+0.51	0.05	15.77	22.73
42	00 26 07	-23 55 04	65.8	-83.8	3	5	I	0.1087	15.87	+0.64	0.02	16.09	20.97
43	00 26 17	+17 18 29	115.3	-45.0	0	4	III:	0.1114	16.64	+0.73	0.04	16.87	21.69
77	00 37 48	+29 16 52	120.1	-33.3	1	5	I:	0.0719	15.00	+0.63	0.09	15.24	20.99
98	00 43 52	+20 11 45	121.4	-42.4	3	5	II-III:	0.1033 (1,2)	15.84	+0.69	0.04	16.08	21.06
136	01 01 33	+24 48 57	126.6	-37.7	2	6	I	0.1569	16.57	+0.79	0.09	16.64	20.74
140	01 02 09	-24 14 35	166.9	-85.7	3	6	II:	0.1591	16.44	+0.72	0.02	16.55	20.63
160	01 10 21	+15 13 39	130.6	-47.1	0	4	III	0.0442	14.30	+0.64	0.06	14.67	21.47
186	01 20 19	-10 39 39	148.3	-71.7	1	5	II	0.1066	15.47	+0.64	0.05	15.67	20.59
279	01 53 43	+00 48 07	154.5	-57.8	1	5	I-II	0.0797	15.12	+0.61	0.02	15.41	20.94
326	02 11 12	-07 22 49	171.0	-62.1	0	5	II:	0.0558 *	14.63	+0.54	0.02	14.94	21.24
410	03 01 28	+03 32 13	174.1	-45.6	1	5	II	0.0897	16.59	+0.71	0.13	16.76	22.04
423	03 08 55	-12 19 12	195.3	-54.0	2	5	III	0.0797 *	15.54	+0.65	0.09	15.77	21.30
458	03 43 52	-24 27 15	218.9	-50.8	2	5	I-II:	0.1050	15.73	+0.67	0.02	15.98	20.93
545	05 30 05	-11 34 40	214.6	-22.7	4	5	III	0.154 (2)	17.81	+0.88	0.49	17.46	21.60
655	08 21 57	+47 17 47	172.7	+35.2	3	5	I-II	0.1245 (3)	15.64	+0.77	0.07	15.82	20.41
665	08 26 18	+66 00 41	149.8	+34.7	5	6	III:	0.1832 (1)	17.34	+0.88	0.06	17.37	21.15
733	08 57 48	+55 51 13	161.5	+40.3	1	6	I:	0.1159	15.72	+0.75	0.02	15.97	20.71
777	09 23 32	+78 30 19	133.8	+34.2	4	6	III	0.224 (3)	17.91	+0.90	0.00	17.87	21.23
819	09 29 37	+09 54 14	223.5	+40.0	0	5	III	0.0759	15.11	+0.67	0.04	15.42	21.05
858	09 40 41	+06 08 33	229.6	+40.6	0	5	II	0.0881	15.54	+0.75	0.04	15.84	21.17
882	09 48 43	+08 33 14	228.1	+43.5	0	5	I	0.1408	16.43	+0.69	0.03	16.58	20.91
910	09 59 12	+67 24 53	143.6	+42.6	4	6	II-III	0.2055	17.54	+0.95	0.06	17.51	21.05
1018	10 25 19	+17 49 23	221.5	+55.6	1	6	III	0.297 P	18.49	+1.09	0.04	18.24	21.02
1081	10 42 04	+35 47 29	187.7	+61.8	2	5	II-III	0.1588	16.34	+0.74	0.02	16.46	20.54
1123	10 52 59	+75 46 27	131.9	+39.6	2	5	III	0.1235	16.27	+0.79	0.07	16.46	21.06
1149	11 00 23	+07 52 18	245.1	+57.7	0	4	III	0.0710	15.13	+0.63	0.04	15.43	21.21
1155	11 01 55	+35 29 52	186.7	+65.9	0	5	II-III:	0.0738	15.56	+0.60	0.02	15.86	21.56
1169	11 05 01	+44 10 55	167.3	+63.3	1	5	III:	0.0582	15.26	+0.58	0.00	15.62	21.82
1170	11 04 56	+08 15 56	246.0	+58.8	2	6	III	0.1620	16.99	+0.82	0.04	17.10	21.13
1190	11 08 58	+41 07 06	172.8	+65.4	2	5	II:	0.0794	15.36	+0.63	0.00	15.69	21.23
1224	11 18 02	+36 44 41	181.3	+68.7	1	6	II	0.2897	18.32	+1.37	0.02	18.11	20.92
1227	11 18 52	+48 19 14	156.8	+62.8	2	5	II-III	0.1117	16.08	+0.67	0.00	16.33	21.15
1235	11 20 39	+19 52 40	228.7	+68.5	2	5	II:	0.1036	15.90	+0.77	0.00	16.22	21.19
1264	11 24 25	+17 24 14	235.7	+68.1	2	5	III:	0.1267	16.57	+0.68	0.02	16.76	21.31
1346	11 38 38	+06 00 44	261.8	+62.9	1	5	II-III	0.0970	15.82	+0.63	0.02	16.07	21.19
1373	11 42 58	-02 10 26	272.1	+56.4	2	5	III	0.1314	17.12	+0.66	0.04	17.27	21.75
1401	11 49 13	+37 32 20	170.4	+73.9	3	5	III	0.1670	17.58	+0.75	0.00	17.70	21.67
1413	11 52 45	+23 40 49	226.2	+76.8	3	5	I	0.1431	16.16	+0.83	0.02	16.35	20.65
1461	12 01 53	+42 50 24	151.7	+71.8	0	5	II-III:	0.0538	14.85	+0.56	0.00	15.21	21.58
1514	12 15 26	+20 57 01	251.3	+80.0	3	6	III	0.1995	17.51	+0.87	0.04	17.51	21.11
1548	12 26 24	+19 42 29	267.9	+80.7	3	6	I-II	0.1608	16.54	+0.83	0.05	16.65	20.70
1559	12 31 06	+67 24 19	125.7	+49.9	1	5	II	0.1042	15.43	+0.67	0.01	15.69	20.66
1589	12 38 49	+18 50 59	287.2	+81.1	0	5	II-III:	0.0699	14.78	+0.63	0.02	15.10	20.92
1630	12 49 21	+04 50 57	303.2	+67.5	1	5	II-III	0.0649	14.88	+0.65	0.02	15.24	21.21

TABLE 1—*Continued*

Abell	R.A. 1950.0 Dec	l	b	R	D	BM	z		r	g-r	Gal Abs	G I	RAM
1674	13 00 52 +67 44 53	121.3	+49.6	3	5	II-III	0.1055		16.08	+0.66	0.01	16.33	21.27
1689	13 08 57 -01 04 30	313.4	+61.1	4	6	II-III	0.1784	*	17.07	+0.84	0.02	17.15	20.98
1738	13 23 16 +57 51 36	114.2	+59.0	2	5	I:	0.1146		15.55	+0.68	0.00	15.80	20.56
1785	13 42 42 +38 22 53	80.8	+74.3	2	5	I-II	0.0792		15.41	+0.62	0.01	15.73	21.27
1825	13 55 40 +20 52 36	13.4	+73.5	0	4	III	0.0632		15.00	+0.55	0.03	15.29	21.32
1827	13 55 47 +21 54 59	16.8	+73.9	1	5	II:	0.0668		14.87	+0.66	0.02	15.22	21.14
1880	14 10 36 +22 33 10	22.8	+70.9	1	5	III	0.1413		16.40	+0.70	0.02	16.56	20.88
1918	14 24 08 +63 25 06	106.4	+50.8	3	6	I-II	0.1415		16.34	+0.75	0.00	16.53	20.85
1921	14 27 05 +23 19 57	28.1	+67.5	1	5	II	0.1352		16.56	+0.75	0.03	16.75	21.16
1934	14 31 12 +29 40 20	44.9	+67.5	3	6	II	0.2195	P	16.87	+0.86	0.00	16.84	20.24
1940	14 33 55 +55 20 53	96.1	+56.2	3	5	III	0.1393		16.37	+0.76	0.00	16.57	20.92
1984	14 50 24 +28 10 06	41.8	+63.2	2	5	II	0.1231	*	16.00	+0.77	0.04	16.21	20.82
2036	15 08 52 +18 13 14	24.6	+56.6	0	4	II-III	0.1163		16.24	+0.65	0.04	16.43	21.16
2110	15 37 51 +30 52 29	48.8	+53.2	1	5	I-II	0.0978		15.70	+0.67	0.04	15.94	21.04
2125	15 40 48 +66 25 23	101.1	+43.0	4	6	II-III	0.2465	(3)	17.46	+1.04	0.04	17.33	20.50
2184	16 19 46 +50 20 25	77.9	+44.3	0	4	III:	0.0550		15.20	+0.59	0.00	15.57	21.90
2218	16 35 40 +66 19 00	97.8	+38.1	4	6	II:	0.1710	(3)	17.21	+0.79	0.04	17.28	21.21
2244	17 00 53 +34 08 06	56.8	+36.3	2	5	I-II:	0.0970		15.50	+0.69	0.04	15.75	20.87
2246	17 00 26 +64 17 28	94.4	+36.2	3	6	II-III	0.225	P	17.55	+0.92	0.02	17.49	20.84
2263	17 21 12 +26 55 59	49.7	+30.3	0	5	II	0.1051		16.29	+0.84	0.08	16.54	21.49
2283	17 44 54 +69 42 43	100.1	+31.1	1	6	I	0.1830		16.94	+0.86	0.08	16.94	20.72
2377	21 43 22 -10 19 30	45.1	-43.2	2	5	II	0.0808		15.53	+0.62	0.06	15.77	21.28
2388	21 51 11 +08 00 49	65.9	-34.3	0	5	II-III	0.0615		15.26	+0.62	0.09	15.52	21.61
2400	21 55 02 -11 38 57	45.4	-46.4	1	5	II:	0.0881		15.50	+0.69	0.06	15.75	21.08
2420	22 07 39 -12 25 04	46.5	-49.5	2	5	I	0.0838		15.26	+0.60	0.06	15.48	20.91
2440	22 21 23 -01 50 12	62.5	-46.4	0	4	II	0.0904		15.61	+0.68	0.07	15.85	21.11
2459	22 34 06 -15 59 50	46.0	-56.8	0	4	III	0.0736		15.34	+0.65	0.07	15.61	21.31
2462	22 36 30 -17 35 52	43.8	-58.0	0	4	I-II:	0.0755	P	15.05	+0.67	0.05	15.35	21.00
2469	22 38 07 +12 03 07	79.9	-39.4	1	5	II:	0.0656		15.40	+0.64	0.09	15.66	21.61
2496	22 48 17 -16 40 20	47.7	-60.1	2	5	I-II	0.1233		15.82	+0.67	0.04	15.99	20.60
2521	22 59 32 -22 17 35	38.6	-64.7	2	5	I	0.1359	*	16.06	+0.72	0.03	16.24	20.64
2554	23 09 41 -21 46 36	41.5	-66.8	3	5	II:	0.1060	(3)	15.89	+0.63	0.03	16.11	21.04
2559	23 10 27 -13 53 29	58.5	-63.4	1	5	I-II	0.0796		15.28	+0.60	0.03	15.55	21.09
2597	23 22 45 -12 23 57	65.4	-64.9	0	5	III	0.0826		15.55	+0.58	0.03	15.81	21.26
2622	23 32 32 +27 05 42	102.8	-32.5	0	4	II-III:	0.0621		14.69	+0.63	0.08	14.96	21.03
2645	23 38 43 -09 17 44	77.2	-65.5	4	6	II-III:	0.246	(3)	17.76	+1.10	0.04	17.64	20.81
2686	23 56 45 -21 03 34	58.2	-76.5	1	5	II	0.1124	R	16.04	+0.70	0.02	16.28	21.08
2694	23 59 50 +08 07 13	102.7	-52.5	3	5	I:	0.0958		15.14	+0.55	0.08	15.28	20.43

*Redshift is mean of two close, roughly equal components.
P, Redshift obtained with PFUEI/CCD.
R, Redshift obtained with Reticon.
REFERENCES.—(1) Sargent 1973. (2) Sandage, Kristian, and Westphal 1976. (3) Kristian, Sandage, and Westphal 1978.

LVDB) catalog of Abell (1958) clusters. All clusters with richness class 3 or greater and $|b| > 30°$ were selected (excluding those in HGT). Abell 545, a richness 4 cluster at somewhat lower latitude, was included as well. For richness classes 0 to 2, the LVDB magnitudes were restricted to lie in the range 14.2–15.5. Twenty clusters in each of these richness classes were randomly selected subject to these criteria. These procedures result in a selection of poor (richness 0, 1, and 2) clusters considerably brighter and nearer than the rarer very rich ones. The penalty for this is that photometric and metric trends with richness are inevitably contaminated by seeing effects (which we feel we deal with quite accurately) and by cosmological model dependences which cannot in principle be dealt with. The cosmological effects for this sample, however, are very small. Choosing a sample homogeneous in distance would have been preferable but would have required an unacceptable increase in observing time. Hereafter this group of clusters will be designated as the "richness sample."

The clusters were identified from enlargements of POSS-E prints and the positions given in LVDB. In most cases the cluster was obvious, and an improved position of the brightest galaxy was measured. In a few instances (primarily the richness 0 clusters) no cluster was evident, so the galaxy nearest to the LVDB position was chosen (see § II). The initial galaxy selected for clusters 1081, 1934, 2246, and 2686 were actually foreground spirals. The correct objects were found from inspection of direct image data obtained on the field. Table 1 gives a summary of the richness sample. The positions are for the chosen brightest galaxy in each cluster, and are accurate to 15″. In all but four cases, the redshifts listed in Table 1 refer to the brightest cluster galaxy. For clusters 1190, 1689, 1825, and 2377 it was discovered that a nearby galaxy (within 90″) was brighter than the initial selection by ~ 0.07 mag. Galactic coordinates, Abell richness and distance classes, and Bautz-Morgan (1970) types are listed in successive columns. Throughout this paper all dimensions are calculated assuming $H_0 = 60$ km s^{-1} Mpc^{-1} and $q_0 = 0.5$.

The redshifts and photometry of the brightest cluster galaxies are described in §§ II and III. Section IV presents a photometric system suited for cosmological investigations with ground-based CCDs. The properties of these galaxies and the implications for the Hubble diagram are discussed in § V. The structure of the brightest three galaxies in these clusters is discussed by Schneider, Gunn, and Hoessel (1983, hereinafter Paper II); the luminosity function of the cores of 60 of the clusters and a new definition of cluster richness is presented in Schneider (1983).

II. REDSHIFTS

Spectra of the first-ranked galaxy candidates were acquired using a multitude of detection systems during 1979–1981. Table 2 is a journal of spectroscopic observations giving the relevant instrumentation parameters. Detailed descriptions of the detectors can be found in Schechter and Gunn (1979) [SIT]; Gunn and Westphal (1981) [CCD]; and Young, Schneider, and Shectman (1981) [Reticon]. The exposures were generally 400 s in length, except for the 1.5 m data where integrations of 2000–4000 s were required. Most of the observations were made through a 2″ slit; the slit width for the CCD system was 1″.5. Observing conditions ranged from nearly overcast to photometric; the seeing, from 1″ to 8″. Figure 1 displays examples of spectra taken with the various systems.

Wavelength calibration was performed using He or He/Ar lamps. The reduction process for the SIT spectra is very similar to that given in Schneider and Gunn (1982). After processing to one-dimensional data, the spectra were rebinned on a logarithmic wavelength scale (bin sizes of 350 km s^{-1} and 200 km s^{-1} for the low- and high-resolution data) and cross-correlated with two radial velocity templates (K giants) using the Fourier quotient technique of Sargent *et al.* (1977). Redshifts for the CCD and Reticon data were measured directly from plots of the spectra. The adopted redshifts of all 84 clusters are given in Table 1. The velocities have a solar motion term of 300 sin l cos b removed. The redshifts for nine clusters were taken from the literature; they are identified in Table 1 by a reference number in parentheses following the redshift.

TABLE 2

SPECTROSCOPIC DATA SYSTEMS

Telescope (inches)	Detector	Dispersion (Å mm^{-1})	Pixel Size (μm)	Resolution (Å)	Clusters
200	SIT	295	23	9	63
200	SIT	140	23	5	7
200	CCD	435	15	25	1
60	CCD	435	15	35	3
200	Reticon	17	30	2	1
Literature					9

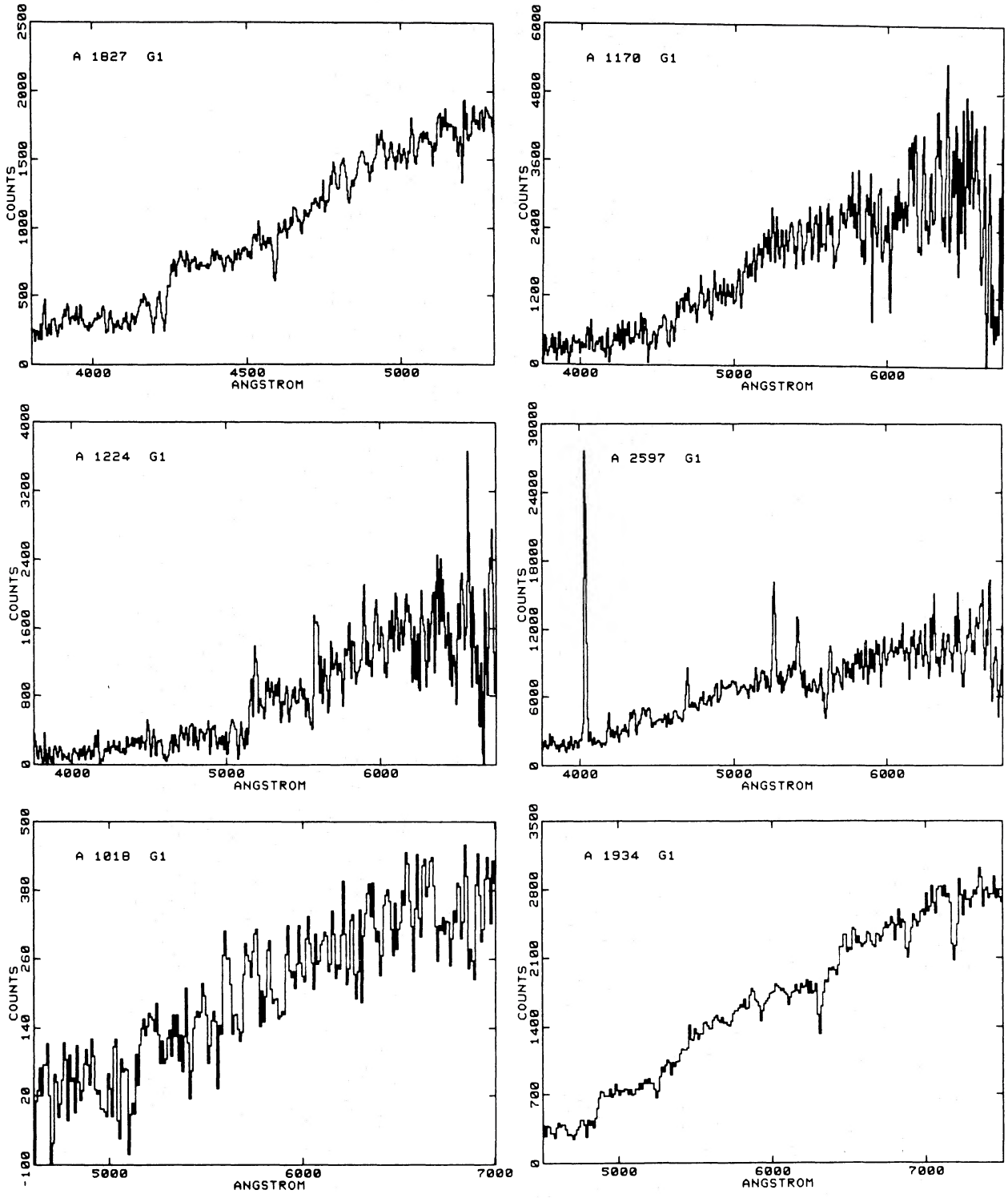

FIG. 1.—A tableau of six brightest cluster galaxy spectra, all on a linear flux scale, with 1 DN = mag 25.0. The observations were made through either a 1".5 or a 2" slit. The data have been rebinned so that there are roughly two points per resolution element. The top four galaxies were observed with the 5 m SIT spectrograph. The lower two were acquired with the PFUEI/CCD system; A1018 at the Palomar 1.5 m (4000 s), A1934 with the Hale telescope (1000 s). See Table 2 for a summary of the different data systems.

TABLE 3

CLUSTERS WITH MORE THAN ONE GALAXY REDSHIFT

Cluster	Galaxy	*cz*
22	N	43140
	S	42690
160	G1	13260
	4'PA 70	13150
326	NW	16380
	SE	17080
423	E	23760
	W	23980
545	G1	46170
	35"PA 160	48360
882	G1	42210
	10"W	42290
910	G1	61610
	20"W	62290
1123	G1	37040
	8"E	36500
1373	G1	39390
	8'PA 43	36150
1689	E	52490
	W	54470
1880	G1	42340
	10'PA 25	46620
1921	G1	40520
	30"E	41740
1934	G1	65800
	5"W	66310
	38"W	65220
1984	N	36080
	S	37740
2244	G1	29330
	40"E	28280
2521	E	41300
	W	40130

Several checks on the accuracy of the SIT numbers are possible. Redshifts determined using the two templates agreed to ~ 90 km s^{-1} for the high-resolution data; to ~ 100 km s^{-1} for the low-resolution data. Five galaxies were observed at both high and low resolution. The scatter in the velocities was of the order of 100 km s^{-1}. Comparison of nine of our measurements with those of other workers shows agreements on the scale of ~ 300 km s^{-1}. Systematic errors of this order are to be expected considering beam bending (anomalous deflection of the readout beam due to the charge on the target; see Schechter and Gunn 1979) and the lack of comparison lines in the relevant part of the spectrum. The only measurement which is in serious disagreement with previous ones was the redshift for 1689. Our value is over 1000 km s^{-1} larger than that of Humason, Mayall, and Sandage (1956, hereafter HMS). Both measurements refer to the mean of two close components. A comparison of finding charts, however, indicates that our eastern galaxy is composed of two condensations; the measurement of HMS refers to the average of these nuclei. The redshift of our eastern component (Table 3) is in good agreement with the values of HMS. Measurement of several features in the CCD and Reticon spectra have an internal consistency of ~ 250 km s^{-1}.

Table 3 lists clusters that had more than one member's redshift measured. This was usually the result of a companion accidentally falling on the slit. In a few cases an effort was made to observe galaxies which had luminosities comparable to the designated brightest one. For clusters that had two close (< 10") equal components, the cluster redshift was taken as the mean of the two. Usually these components differed by only several hundred km s^{-1}, but the pair in 1689 have a velocity difference of 2000 km s^{-1}. Cluster redshifts which are the mean of two components have their redshifts followed by an asterisk. A *P* after the entry indicates the observation was performed with the CCD system, an *R* denotes the Reticon observation.

Figure 2 displays a histogram of the redshifts broken down by richness class (the HGT clusters are also plotted). It is clear that Abell richness class and distance are rather correlated in the richness sample. There are two surprises—1018 and 1224. These seemingly innocuous richness 1 clusters are at redshifts of nearly 0.3, which is near the limit of the Abell catalog. (The largest

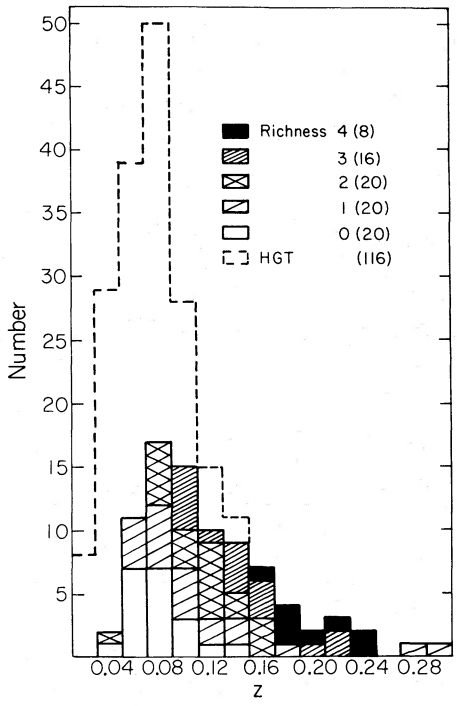

FIG. 2.—A histogram of the redshift distribution for the 200 low-redshift clusters. The dotted line represents the galaxies in HGT; the richness sample clusters are coded by richness class. The correlation of richness with redshift in the richness sample is evident.

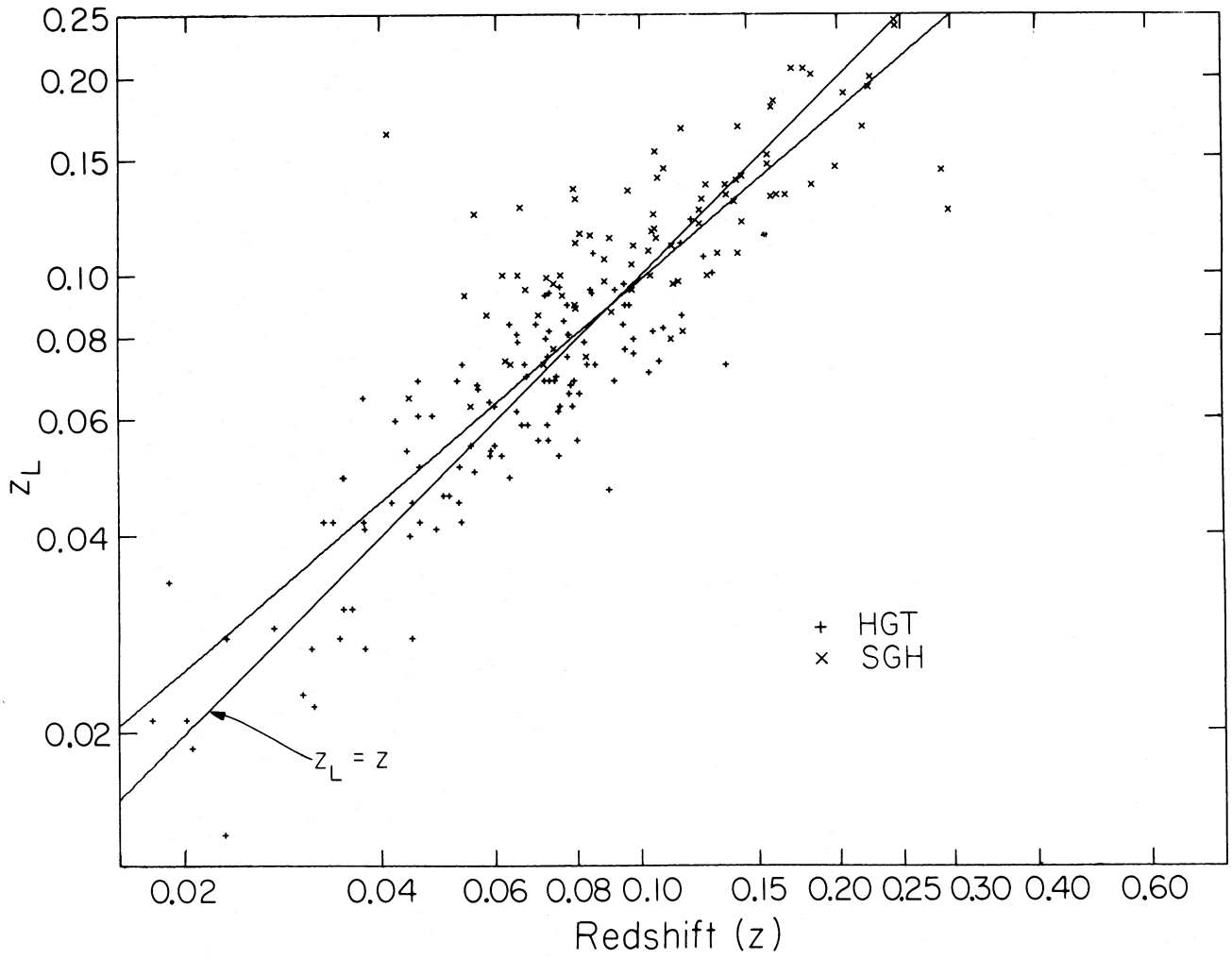

FIG. 3.—A comparison of the redshifts from Leir and van den Bergh (1977) [z_L] with those of HGT (+) and the richness sample (×). One solid line is $\log z = \log z_L$, the other is the best linear fit: $\log z = 1.18 \log z_L + 0.18$. The regression line indicates an accuracy in z_L of ~ 25%. See text for discussion.

known redshift for an Abell cluster is 0.373 for 370, see KSW.)

Some interesting insights can be drawn by relating these numbers to the redshift estimates of LVDB, who estimated cluster distances based on the appearance of the brightest galaxy and various cluster properties. Comparison with ~ 100 published cluster redshifts indicated an accuracy of ~ 20%. Figure 3 is a plot of the LVDB velocities versus those of HGT and Table 1. Two lines are plotted, a line of unit slope passing through the origin and the best fitting straight line. The flattening of the relation may be due to selection effects—as one proceeds to higher redshift (more volume), one encounters more diverse cluster types (including rare, rich ones which stand out). Placing the distant clusters on the same relation as nearby ones may skew the relation, causing a distance underestimate for the distant clusters and an overestimate for the nearby ones. It is likely, however, that we are simply overinterpreting this effect; Figure 3 shows that the line with unit slope fits almost as well.

Some of the scatter is due to problems of identification and/or catalog error, since in some instances there is no obvious cluster at the catalog position. For example, no cluster is found at the position of 2516, which was in the richness sample originally. In this obvious case, another cluster, 279, was drawn from the pool to replace it. Rather more serious is the case of Abell 34, which is at one-quarter of its LVDB distance. There were only two other "cluster" members on the CCD frame; there is no doubt that the object is not a cluster at all, and it was excluded in the analysis. Notice that there is no danger of bias from this arbitrary procedure. The "brightest galaxy" in the cluster stands four stan-

dard deviations from the Hubble line, and the cluster would in any case never have been selected in the distant samples to be used for cosmological tests.

One of the clusters, 2597 (see Fig. 1), has a remarkable emission-line spectrum. It is the only one of the brightest cluster galaxies that shows any emission lines. The galaxy was identified with the radio source PKS 2322−12 (Schmidt 1965), and has a radio luminosity of 6×10^{42} ergs s^{-1}. A search of a radio source list (Dixon 1970) found 13 other radio sources within 2.5 of a position in Table 1. The resulting radio luminosities range from $2\text{–}40\times10^{41}$ ergs s^{-1}. This is roughly 30% of the clusters in the richness sample in the relevant redshift range (< 0.14). Richness classes 0, 1, 2, and 3 were represented. No richness 4 clusters have radio counterparts, but then the nearest (545) is more distant than any of the radio clusters.

III. PHOTOMETRY

Direct imaging of the central few arcminutes of each cluster was obtained with the PFUEI/CCD system. Observations were made in the g and r filters of Thuan and Gunn (1976), and the instrumental magnitudes transformed to this system from observations of six to twelve photometric standards each night. Typical residuals in the r magnitude were 2–2.5%; they never exceeded 4%. Difficulty was experienced on some nights with the g photometry, a phenomenon almost certainly connected with ill-understood effects in the "dead layer" in the unpassivated silicon surface of the CCD. The residuals on these nights often change systematically in the sense that the detector becomes less sensitive with time. This behavior can be compensated given enough standards; this has been done.

CCDs are truly marvelous detectors, but they do have one troublesome property—their wavelength response is so different from photoemissive devices that it is difficult to tie broad-band photometry to existing systems based on photomultipliers. This presents a serious problem to us, as we wish to compare the observations in this paper with the photocathode results in HGT. We have decided to handle this problem in an inelegant but practical way. The Thuan-Gunn (TG) g and r magnitudes for the standards were adopted; the transformations of the CCD data to these numbers work well for stars with $-0.8 < (g-r)_{TG} < +0.9$. Standards with $(g-r)_{TG} > 1.0$ had transformation $(g-r)$'s which were over 0.1 mag redder than the TG values (several photomultiplier measurements were kindly communicated to us by S. Kent), and were ignored when deriving the final photometric transformations. The red star discrepancy is not unexpected, as M stars have complex spectra which play havoc with attempts to move between broad-band photometric systems. See the end of § IV for a discussion of this problem.

The measurements of the brightest cluster galaxies are given in Table 1. These are the observed magnitudes based on the above transformations. The magnitudes refer to the light inside a 16 kpc radius in the $q_0 = 0.5$, $H_0 = 60$ model. For the more distant clusters this radius is less than 4″, and atmospheric seeing (usually 1.″1–1.″7) cannot be ignored. The adopted seeing correction procedure is described in Paper II. Briefly, the seeing profile was determined from a star on the frame (a suitable candidate could always be found); then the radial profile of the galaxy was fitted to both a de Vaucouleurs law and a modified Hubble model

$$I(x) = \frac{I_0}{\left[1+(x/a)^2\right]^{0.9}}, \qquad (1)$$

each convolved with a double Gaussian fit to the seeing (the 0.9 in the Hubble profile comes from the mean slope in the region around 16 kpc in brightest cluster galaxies; see Paper II). A 16 kpc correction factor was calculated and then applied to the actual aperture measurement. This correction was usually negligible, only rising to 0.025 mag for the most distant clusters.

Photometric data on all the clusters were obtained with the 1.5 m system (see Schneider and Gunn 1982 for a description) between 1979 August and 1980 August. Half of the photometric measurements were in very poor seeing; these clusters were redone on nights with good seeing ($< 1.''5$). The nonphotometric good seeing pictures (r filter, 500–1500 s exposures) were tied to the photometric ones by comparing multiaperture magnitudes for the brightest galaxy. This was tested with clusters which had photometric data with good and bad seeing. These galaxies had magnitudes consistent to 0.04 mag. The only problems arose with a few of the most distant clusters which had uncertainties of 0.07 mag, probably because, unlike the case for the nearby clusters, the apertures could not be made many times larger than the seeing disk.

Hoessel (1980) found that ~ 30% of first-ranked cluster galaxies were multiple-nucleus systems; i.e., more than one "galaxy" occurred within the 16 kpc aperture (for an extreme example of this, see Schneider and Gunn 1982). Because of the ambiguity of what constitutes a "galaxy" in multiple systems, we shall adopt as a working definition of the brightest cluster galaxy *the region of maximum light enclosed in an aperture with a radius of 16 kpc*. The second and third brightest cluster galaxies are defined in an analogous way. This procedure has several practical advantages—including objectivity and algorithmic simplicity with linear image data. It also can be applied to clusters at vastly different redshifts. The drawback, as is readily seen in Schneider and Gunn (1982), is that the resulting profiles can be very bizarre (see Paper II for a discussion). The profiles

for the most extreme of these systems are, of course, fitted very poorly by either modified Hubble or de Vaucouleurs laws, but this procedure has the enormous advantage of not introducing distance-dependent biases. One has the option of rejecting extreme cases through the α-parameter, which is determined in a roughly seeing-independent way.

The $(g-r)$ colors were measured by comparing the integrated colors in several apertures with radii of ~ 16 kpc. Errors in the sky subtraction manifest themselves by rapid changes of color with radius; in nearly all our data on brightest galaxies, the internal consistency was $\sim 2\%$ in the 12–18 kpc range. Approximately 20 clusters had photometric measurements taken on different nights. These observations were obtained with different CCDs and slightly different g filters. Despite the dissimilarity of the photometric transformation equations, 80% agreed to 0.03 mag. The galaxies with large residuals were reobserved.

IV. A STANDARD COSMOLOGICAL PHOTOMETRIC SYSTEM

In this paper we present observations in only the g and r passbands, but wish to include two other filters in the following discussion of photometric data processing; i (Wade *et al.* 1979), and z (this paper). These last two filters are required for observations of high-redshift clusters, so that one can observe near a given wavelength in the rest frame of the galaxy. This system has several advantages for ground-based CCDs. The filters span the response range of this detector (4500–11000 Å), and several strong sky lines are avoided (Hg 4358 and 5460, and [O II] λ5577). The z filter consists of 3 mm of RG 850 (50% of peak transmission at 8400 Å, peak transmission of 93% reached at 10200 Å), one reflection off aluminum, and the prime focus universal extragalactic instrument (PFUEI) plus a Texas Instruments 800×800 CCD. The response curves for the PFUEI can be found in Gunn and Westphal (1981). The relative response curve of the *griz* system are shown in Figure 4; all factors except atmospheric extinction have been included.

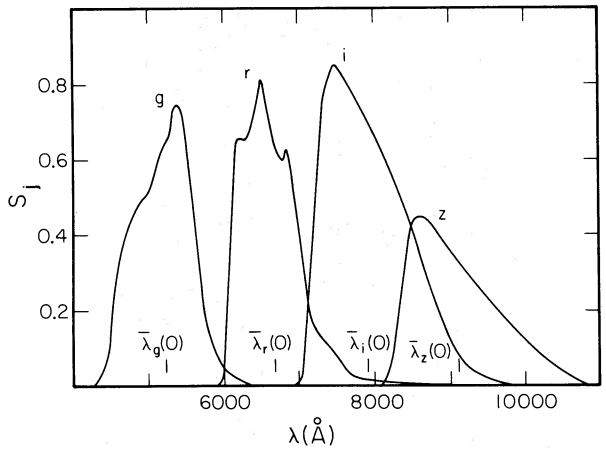

FIG. 4.—The transmission function $S(\nu)$ for the bandpasses of the *griz* system, PFUEI, and one reflection from aluminum.

The clusters (except for A545) have been restricted to galactic latitudes greater than 30° to minimize galactic obscuration. Sandage (1973) found that the absorption could be represented by a csc b law; however, it is clear that there are local inhomogeneities in the reddening (Heiles 1975). Absorption corrections based on the intervening neutral hydrogen density are likely to be more accurate than corrections determined from galactic latitude alone.

From van de Hulst's curve 15 (Johnson 1968)

$$A(g)=3.29E(B-V),$$
$$A(r)=2.23E(B-V),$$
$$A(i)=1.63E(B-V),$$
$$A(z)=1.22E(B-V). \quad (2)$$

Burstein and Heiles (1978) present a comprehensive study of galactic reddening as a function of the column density of neutral hydrogen. We selected their observations with $|b|>30°$ and $N_H<400$ (N_H is the column density of neutral hydrogen/2.23×10^{18}, which is the unit used in the contour maps of Heiles 1975), and executed a linear fit to 46 points which gave

$$E(B-V)=1.90\times10^{-4}\,(N_H-68.9),$$

rms scatter in $E(B-V)=0.026$.

Note that the absorption becomes zero at a nonzero value of the column density. This phenomenon is in part due to the presence of emission from the galactic plane in the dish sidelobes, but perhaps not entirely (see Stark and Heiles 1981). Its origin is not of primary interest to us, since we wish to use the Heiles contour maps only as an interpolation device for the reddening. Defining

$$N'=N_H-68.9;$$

for a galaxy at rest

$$A(g)=6.24\times10^{-4}N',$$
$$A(r)=4.23\times10^{-4}N',$$
$$A(i)=3.09\times10^{-4}N',$$
$$A(z)=2.31\times10^{-4}N'. \quad (3)$$

For galaxies at nonzero redshifts, the absorption is

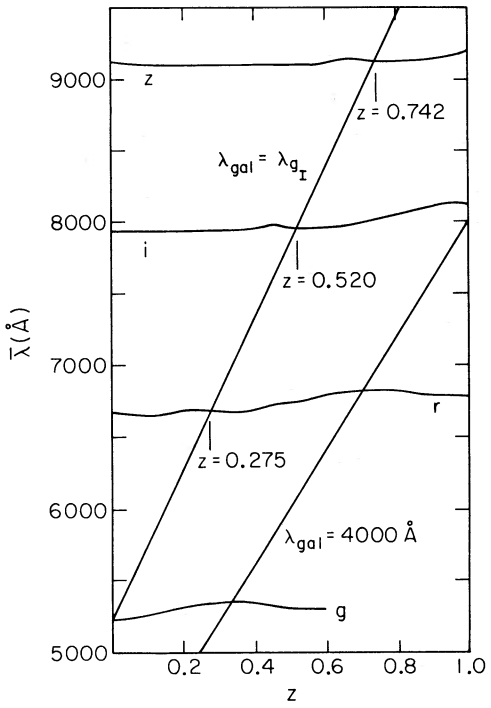

FIG. 5.—Effective wavelengths of the griz filters for first-ranked cluster galaxies. Diagonal lines represent the positions of the effective wavelength of g_I ($= g$ at $z = 0.0$, $\bar{\lambda}_{g_I} = 5242$ Å) and the "break" at 4000 Å. This system allows interpolation for g_I up to a redshift of 0.74.

calculated by interpolating in the above formulae using the effective wavelength of the filter (see Fig. 5). If the column density becomes greater than 400 (for 545, for example), the color excess is read from the $E(B-V)$ versus $N_{\rm H}$ graph of Burstein and Heiles (1978), and the absorption calculated from (2). The polar reddening is known to be small (Sandage 1973), and these formulae result in essentially no absorption at the poles. The galactic absorption in the red band for each cluster is listed in Table 1. The same absorption correction procedure was applied to the HGT sample. Two of the HGT clusters have small negative galactic absorption with this scheme, $A(r) = -0.002$ mag ($N_{\rm H} = 65$); none of the richness clusters had negative absorption. This procedure is open to a good deal of improvement, as the errors in the r magnitude induced by uncertainty in the reddening are 0.06 mag.

We now turn to the problem of correcting the observations for redshift related effects (the fact that one observes a different portion of the spectrum as the redshift increases), and propose a slightly new way of handling this problem. We note that the detectors employed are photon-counting systems, not energy sensitive devices. (The same is true, of course, of photomultipliers; our new definition of the k-correction is the correct one for all such detectors.) For each filter (j) define $S_j(\nu)$ to be the probability that a photon of frequency ν will be detected by the system. This folds in filter and atmospheric (airmass 1.2) transmission, reflectivity of aluminum, and response of the detector. (Note that the response curves in Fig. 4 do not include the atmospheric transmission factor.) The apparent magnitude m_j is defined as

$$m_j = C_j - 2.5 \log \left[\int_0^\infty n_\nu S_j(\nu)\, d\nu \right],$$

n_ν = number of photons of frequency ν incident on atmosphere s^{-1} cm^{-2} Hz^{-1},

C_j = constant found from photometric standards.

The absolute magnitude of an object is

$$M_j = C_j - 2.5 \log \left[\frac{\int_0^\infty N_\nu S_j(\nu)\, d\nu}{4\pi D_0^2} \right] \quad (D_0 = 10 \text{ pc}).$$

The photon flux from an object at redshift z is

$$n_\nu = \frac{N_{\nu(1+z)} H_0^2}{4\pi c^2 Z_q^2(z)} = \frac{N_{\nu(1+z)}(1+z)^2}{4\pi D_L^2},$$

where

$$Z_q(z) = \frac{1}{q_0^2(1+z)} \left\{ q_0 z + (q_0 - 1)\left[(1+2q_0 z)^{1/2} - 1 \right] \right\},$$

and

$$D_L = \text{luminosity distance} = \frac{c Z_q(z)(1+z)}{H_0}$$

(Weinberg 1972). Thus

$$m_j = C_j - 2.5 \log \left[\int_0^\infty \frac{N_{\nu(1+z)}(1+z)^2 S_j(\nu)\, d\nu}{4\pi D_L^2} \right]$$

or

$$m_j = M_j - 5 \log \frac{D_0}{D_L} + 2.5 \log \left[\frac{1}{(1+z)^2} \frac{\int_0^\infty N_\nu S_j(\nu)\, d\nu}{\int_0^\infty N_{\nu(1+z)} S_j(\nu)\, d\nu} \right].$$

Define the k-correction $k_j(z)$ as

$$k_j(z) = 2.5 \log \left[\frac{1}{(1+z)^2} \frac{\int_0^\infty N_\nu S_j(\nu)\, d\nu}{\int_0^\infty N_{\nu(1+z)} S_j(\nu)\, d\nu} \right]$$

$$= 2.5 \log \left[\frac{1}{1+z} \frac{\int_0^\infty (f_\nu/\nu) S_j(\nu)\, d\nu}{\int_0^\infty (f_{\nu(1+z)}/\nu) S_j(\nu)\, d\nu} \right].$$

The absolute magnitude is

$$M_j = m_j - 5 \log D_L - 25 - k_j(k) \quad (D_L \text{ in Mpc}).$$

Following GO, we shall define the reduced absolute magnitude (RAM) as

$$\text{RAM}_j = M_j + 5 \log [c/H_0] - 5$$

or

$$\text{RAM}_j = m_j - 5 \log [Z_q(z)(1+z)] - k_j(z).$$

This quantity removes the effects of H_0 on the absolute magnitudes. The meaning of the reduced absolute magnitude is easily visualized; it is the k-corrected apparent magnitude of an object placed at a luminosity distance of one Hubble radius. In our model, $R_h = c/H_0 = 5000$ Mpc, $z_{R_h} = 0.866$, and the distance modulus $5 \log R_h - 5 = 43.49$ mag. The formalism thus far is very similar to those of past investigators (Sandage 1961; GO; SKW; KSW; HGT) except for the definition of the k-correction. Basing the k-correction on photons instead of energy does result in differences of up to 0.015 mag when sharp features (the 4000 Å break) enter the filter bandpass. In these instances the photon k-corrections are smoother than the energy ones; this is because the detector sees a big drop in the high-energy photons which carry a larger fraction of the detected energy than the detected number of photons.

In order to construct a Hubble diagram, a passband in the rest frame of the galaxy must be selected. One wants to chose one at the blue end so it is accessible at high redshift, but not so blue that line blanketing will render the magnitude sensitive to metallicity. The g filter is an excellent compromise for our system, as the detector is insensitive at shorter wavelengths and redshifts greater than 0.74 are required to push g out of our observational range. Hereafter g_I will represent this standard magnitude.

For historical reasons (GO) we will define

$$g_I = C_g - 2.5 \log \left[\int_0^\infty \frac{f_\nu}{\nu} S_g[\nu(1+z)]\, d\nu \right],$$

$$g_I = m_g - k_g(z) - 2.5 \log (1+z).$$

The $(1+z)$ term makes g_I behave like a monochromatic magnitude; it is roughly the monochromatic magnitude at the redshifted wavelength which corresponds to the center of the g band in the galaxy rest frame. Note the $g_I = g$ at $z = 0$.

If all galaxies had the same spectral shape, an observation in a single filter would suffice to obtain the magnitude in a preselected bandpass. HGT presented a method in which observations were obtained in two filters which bracketed the position of the desired wavelength region. We will adopt their procedure with a few minor modifications.

One needs to know the effective wavelengths for the various filters; this, however, is an ill-defined problem for any filter of finite width. We define the effective frequency for a given filter as

$$\nu_{j,\text{eff}} = \hat{\nu}_j = \exp \left[\frac{\int_0^\infty n_\nu S_j(\nu) \ln \nu\, d\nu}{\int_0^\infty n_\nu S_j(\nu)\, d\nu} \right],$$

where n_ν is a fiducial source, in our case NGC 4889. Notice that this definition is in a sense halfway between an effective frequency and an effective wavelength, and is chosen over those purely for aesthetic reasons. As the object moves to higher redshift,

$$\bar{\nu}_j(z) = \exp \left[\frac{\int_0^\infty n_{\nu(1+z)} S_j(\nu) \ln \nu\, d\nu}{\int_0^\infty n_{\nu(1+z)} S_j(\nu)\, d\nu} \right]$$

and

$$\bar{\lambda}_j(z) = \frac{c}{\bar{\nu}_j(z)}.$$

Figure 5 displays the redshift dependence of the effective wavelength in the *griz* system. One diagonal line is the position of the effective wavelength of our selected passband (g_I), the other is the "break" at 4000 Å. As the break enters a given bandpass, the effective wavelength moves to the red.

Let $\hat{\nu}_{g_I}$ = effective frequency of the desired region ($= \bar{\nu}_g(0)$), and filters k and j be the lower and upper (frequency) bounds (selected from Fig. 5). One can calculate a g_I from both the k and j filters applying the appropriate $k(z)$ correction.

$$g_I(j) = m_j - k_j(z) + (g-j)_0 - 2.5 \log (1+z),$$

where $(g-j)_0$ is the color of the standard galaxy at

rest. Then

$$g_I = \frac{\ln\left[\frac{\hat{\nu}_{g_I}(1+z)}{\bar{\nu}_k}\right] g_I(j) + \ln\left[\frac{\bar{\nu}_j}{\hat{\nu}_{g_I}(1+z)}\right] g_I(k)}{\ln\left[\frac{\bar{\nu}_j}{\bar{\nu}_k}\right]}. \quad (4)$$

A small modification in the interpolation equation (4) was adopted in the handling of the richness sample (CCD) data. Double weight was given to the r measurement because of the temporal response variations and associated reduction difficulties in the g band. The HGT data had equal weight given to $g_I(g)$ and $g_I(r)$. For the two clusters in the richness samples that have g_I shifted above the r band, g_I was set equal to $g_I(r)$.

We must now address the problem with the CCD photometric system mentioned in the previous section. The filters used with the PFUEI were convolved with the PFUEI plus CCD response curve, one reflection off aluminum, and the atmospheric transmissivity at 1.2 airmasses. From our CCD photometry and photometric multichannel scans of standards lent us by J. B. Oke, we find

$$r = r_c + 0.044(g-r)_c,$$

$$g - r = 1.199(g-r)_c,$$

$$r - i = 1.127(r-i)_c,$$

$$i - z = 0.925(i-z)_c.$$

The subscript c indicates the natural CCD magnitudes, and the left-hand side represents the adopted *griz* system magnitudes. These magnitudes are equal to the original Thuan-Gunn magnitudes for objects whose spectra are smooth. To understand how galaxies behave with the CCD system, scans of NGC 4889 and the large-aperture composite galaxy of Whitford (1971) were numerically convolved with the photoelectric and CCD response functions. The resulting "natural" CCD colors were then transformed with the linear transformations appropriate to placing the standards on the photoelectric system. The transformed CCD r agreed with the photoelectric r to better than 1% for galaxies with $z < 0.30$. The $(g-r)$ values, however, were discrepant; the photoelectric color was more than 0.15 mag redder than the transformed CCD value at $z = 0.2$. This is due to the changed character of the g filter. In the photoelectric system the filter has $\hat{\lambda}_g = 4947$ Å and reaches down to 4200 Å. The CCD g response is basically dead by 4500 Å, and $\hat{\lambda}_g = 5242$ Å. As the galaxy redshift increases, the photoelectric g sees the "break" much earlier than the CCD g does, and thus the photoelectric colors turn redder. Our system is this linearly transformed "natural" system. It has standard photometry negligibly different from the photoelectric system for the subdwarf standards by which that system is defined. To calculate colors on it from scans, however, one produces natural magnitudes with the CCD response functions and then applies the above transformations. Predicted k-correc-

TABLE 4

FILTER REDSHIFT CORRECTIONS $k(z)$

Redshift	g	r	i	z
0.00	0.00	0.00	0.00	0.00
0.02	0.05	0.02	0.02	0.02
0.04	0.10	0.04	0.04	0.04
0.06	0.16	0.05	0.06	0.06
0.08	0.21	0.07	0.08	0.08
0.10	0.26	0.09	0.09	0.10
0.12	0.32	0.12	0.11	0.11
0.14	0.38	0.14	0.13	0.12
0.16	0.45	0.16	0.15	0.14
0.18	0.52	0.20	0.16	0.15
0.20	0.61	0.24	0.18	0.17
0.22	0.72	0.27	0.19	0.18
0.24	0.83	0.31	0.21	0.20
0.26	0.95	0.34	0.22	0.21
0.28	1.07	0.37	0.24	0.23
0.30	1.18	0.40	0.26	0.25
0.32	1.28	0.43	0.28	0.26
0.34	1.40	0.45	0.30	0.28
0.36	1.51	0.48	0.32	0.30
0.38	1.65	0.51	0.35	0.32
0.40	1.74	0.55	0.37	0.33
0.42	1.87	0.59	0.41	0.35
0.44	1.93	0.65	0.43	0.36
0.46	2.03	0.71	0.46	0.37
0.48	2.09	0.76	0.47	0.38
0.50	2.16	0.82	0.49	0.39
0.52	2.23	0.88	0.50	0.40
0.54	2.28	0.95	0.52	0.41
0.56	2.34	1.03	0.53	0.42
0.58	2.39	1.10	0.54	0.43
0.60	2.43	1.19	0.56	0.44
0.62	...	1.27	0.57	0.46
0.64	...	1.34	0.60	0.48
0.66	...	1.42	0.63	0.50
0.68	...	1.49	0.65	0.52
0.70	...	1.57	0.69	0.53
0.72	...	1.65	0.72	0.54
0.74	...	1.72	0.75	0.55
0.76	...	1.80	0.79	0.56
0.78	...	1.86	0.82	0.57
0.80	...	1.92	0.86	0.58
0.82	...	1.98	0.91	0.60
0.84	...	2.00	0.97	0.62
0.86	...	2.06	1.03	0.65
0.88	...	2.11	1.10	0.68
0.90	...	2.16	1.17	0.71
0.92	...	2.22	1.24	0.74
0.94	...	2.26	1.30	0.78
0.96	...	2.30	1.37	0.83
0.98	...	2.36	1.44	0.87
1.00	...	2.39	1.50	0.91

tions were produced in this fashion and are given in Table 4. Photometric transformations for brightest cluster galaxies (at rest) are

$$g = r + 0.47, \quad B = g + 0.68,$$

$$r = i + 0.31, \quad B = V + 0.97,$$

$$i = z + 0.22, \quad J = V + 0.34,$$

$$r = R + 0.30, \quad J = F + 1.1.$$

(The J and F relations are from Oemler 1974.) For a galaxy at rest, adding 0.06 mag to g will yield the AB magnitude (flux scale of Oke and Schild 1971) at 5000 Å.

The galaxies of HGT were placed on the CCD system by taking the r magnitude (with no change) and setting $(g-r) = (g-r)_{\rm HGT} + \Delta(z)$, where $\Delta(z)$ was found from the previously mentioned scans. The reduced absolute magnitudes for these galaxies are given in Table 5. Nineteen galaxies from GO were also transformed to the CCD system (adopting $g_I = VI + 0.27$ from the scan of NGC 4889); their magnitudes can be found in Table 6. Figure 6 shows the observed $(g-r)$ colors for the brightest cluster galaxies of HGT and the richness sample versus the predictions of Table 4. It is clear that the points are consistent with the existence of a standard galaxy for $z < 0.25$.

V. DISCUSSION

Figure 6, along with a similar plot in KSW, presents reassuring evidence that one can use the k-correction procedure with confidence. For the HGT and the richness clusters the average difference between the observed $(g-r)$ and the calculated one is $+0.008$ mag with a standard deviation of 0.055 [this is reflected in a

TABLE 5

GALAXIES FROM HOESSEL, GUNN, AND THUAN (1980)

Cluster	z	RAM	Cluster	z	RAM	Cluster	z	RAM
21	0.0948	20.63	1216	0.0524	21.53	2022	0.0565	21.16
76	0.0377	21.14	1228	0.0344	21.59	2028	0.0772	20.90
85	0.0556	20.78	1238	0.0716	21.28	2029	0.0777	20.36
88	0.1086	21.10	1254	0.0628	21.39	2040	0.0456	21.71
104	0.0822	21.12	1291	0.0586	21.89	2048	0.0945	20.88
119	0.0446	21.06	1318	0.0189	21.85	2052	0.0351	21.26
147	0.0441	21.54	1364	0.1070	21.13	2061	0.0782	20.73
151	0.0526	20.62	1365	0.0763	21.25	2063	0.0337	21.31
154	0.0612	20.75	1367	0.0205	21.31	2065	0.0722	21.17
166	0.1156	21.57	1377	0.0509	21.31	2067	0.0726	21.56
168	0.0457	21.23	1382	0.1046	21.05	2079	0.0657	20.82
189	0.0349	21.68	1383	0.0598	21.68	2089	0.0743	20.94
193	0.0478	20.90	1399	0.0913	21.41	2092	0.0669	21.45
194	0.0178	20.89	1412	0.0839	21.48	2107	0.0421	20.87
225	0.0692	21.14	1436	0.0646	21.10	2124	0.0671	20.92
246	0.0753	21.59	1468	0.0853	21.35	2142	0.0911	21.30
274	0.1289	20.85	1474	0.0778	21.68	2147	0.0377	21.21
277	0.0947	20.95	1496	0.0961	21.45	2151	0.0360	21.25
389	0.1160	20.90	1541	0.0892	21.05	2152	0.0444	21.32
399	0.0725	21.05	1644	0.0456	21.26	2162	0.0318	21.25
400	0.0231	21.53	1651	0.0842	20.96	2175	0.0978	21.18
401	0.0752	21.05	1656	0.0230	20.67	2197	0.0303	20.75
496	0.0326	21.21	1691	0.0722	20.88	2199	0.0312	20.59
500	0.0666	21.16	1749	0.0562	20.98	2255	0.0747	20.99
514	0.0697	21.34	1767	0.0712	21.00	2256	0.0550	20.58
634	0.0266	21.42	1773	0.0776	20.93	2328	0.1470	20.43
671	0.0497	20.81	1775	0.0718	20.98	2347	0.1196	21.13
779	0.0201	20.92	1793	0.0849	21.34	2382	0.0648	21.44
787	0.1355	20.87	1795	0.0631	21.02	2384	0.0943	21.27
957	0.0437	20.97	1809	0.0788	20.73	2399	0.0587	21.47
978	0.0527	21.05	1831	0.0749	20.80	2410	0.0806	20.97
993	0.0530	20.92	1837	0.0376	21.75	2457	0.0597	20.94
1020	0.0650	21.60	1904	0.0719	20.69	2634	0.0315	20.91
1035	0.0799	20.99	1913	0.0533	21.49	2657	0.0414	22.06
1126	0.0828	20.72	1927	0.0740	21.50	2666	0.0273	20.69
1139	0.0376	21.61	1983	0.0458	21.78	2670	0.0774	20.79
1185	0.0349	20.99	1991	0.0589	21.14	2675	0.0726	21.17
1187	0.0791	20.94	1999	0.1032	21.00	2700	0.0978	20.94
1213	0.0484	21.11	2005	0.1251	20.89			

TABLE 6

GALAXIES FROM GUNN AND OKE (1975)

Cluster	z	RAM
UMa II G1	0.136	21.63
1534+37 G1	0.153	21.45
Hydra G8+G9 ...	0.202	20.67
1604+39	0.235	21.56
0308+16	0.260	21.88
PHL 1093 G2	0.270	21.97
1318+31	0.270	21.40
3C 323 G1	0.270	21.05
1612+42	0.275	21.97
1607+39	0.280	21.23
1021+04	0.286	21.04
1610+41	0.300	21.42
0948+45	0.305	21.41
1049−09 G1	0.330	21.62
0948+44	0.361	21.19
1446+26 G4	0.373	21.41
0024+16 G1	0.380	20.98
0949+44	0.385	21.79
3C 295	0.465	20.43

discrepancy of similar size between $g_I(g)$ and $g_I(r)$]. Since the expected errors in the colors are approximately 0.03 mag (§ III), it is clear that the spectral energy distributions of brightest cluster galaxies are remarkably similar. There is no detectable color evolution in giant ellipticals out to a redshift of 0.25 (~ 3–4×10^9 years).

Table 7 lists the mean absolute magnitudes for the three 16 kpc samples. All three groups indicate that the luminosity of the brightest cluster galaxy has a dispersion of about 0.34 mag, which is similar to the value of SKW and KSW. Tables 8 and 9 and Figures 7 and 8 present the results of binning the HGT and richness samples into richness and Bautz-Morgan classes (BM types from LVDB).

TABLE 7

MEAN REDUCED ABSOLUTE MAGNITUDES

Sample	N	$\langle Z \rangle$	$\langle$RAM$\rangle$	SIG RAM
HGT 1980	116	0.066	21.14	0.33
This paper	83	0.121	21.07	0.35
Gunn and Oke 1975 ...	19	0.291	21.37	0.42

Our data support the tentative conclusion of HGT of an approximately 0.1 mag per richness class brightening of the brightest galaxy from richness class 0 to richness class 3. The richness 4 clusters (plus the one richness 5 one, Abell 665) do not continue this trend, however, this result is significant at the 99% level. In fact, the luminosities of the richness class 4 galaxies fall 0.2 mag below those of richness class 3. SKW found, on the basis of a sample some $2\frac{1}{2}$ times smaller, a change of only 0.05 mag per class. The discrepancy is unlikely to be the result of the difference of aperture sizes used, since the larger aperture of SKW (36 kpc radius) should be more subject to contamination in the rich clusters, which would accentuate the brightening with richness class.

It is important to note that the conclusion regarding the richness effect is not cosmology-independent, since

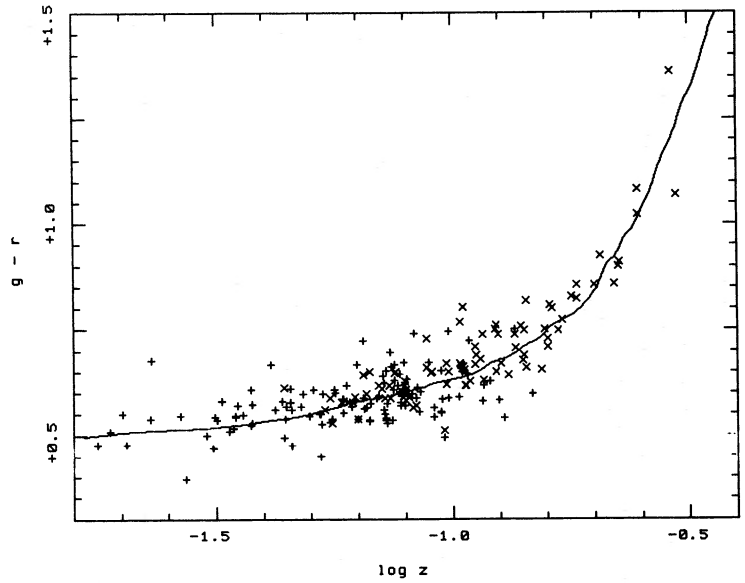

FIG. 6.—The predicted $(g-r)$ colors of first-ranked cluster galaxies as a function of redshift (from a scan of NGC 4889). The observations of HGT (+) and this paper (×) are plotted. The only correction applied to the data is removal of galactic absorption. The observations fit the predicted line quite well: the dispersion is only 0.055 mag.

TABLE 8

RICHNESS CORRECTIONS

Class	N	$\langle Z \rangle$	SIG Z	$\langle$RAM$\rangle$	SIG RAM
			HGT 1980		
0	11	0.035	0.011	21.13	0.31
1	82	0.066	0.022	21.19	0.33
2	21	0.076	0.035	20.96	0.32
3	2	0.103	0.036	20.82	0.04
			This Paper		
0	20	0.079	0.024	21.30	0.27
1	20	0.117	0.067	21.09	0.37
2	19	0.115	0.027	21.02	0.32
3	16	0.146	0.041	20.85	0.35
4	8	0.201	0.035	21.07	0.33
			Total Sample		
0	31	0.063	0.030	21.24	0.29
1	102	0.076	0.041	21.17	0.33
2	40	0.094	0.037	20.99	0.32
3	18	0.142	0.042	20.85	0.33
4	8	0.201	0.035	21.07	0.33

TABLE 9

BAUTZ-MORGAN CORRECTIONS

Class	N	$\langle Z \rangle$	SIG Z	$\langle$RAM$\rangle$	SIG RAM
			HGT 1980		
I	13	0.060	0.022	20.89	0.28
I–II	11	0.061	0.024	21.08	0.31
II	23	0.065	0.032	21.00	0.26
II–III ..	22	0.062	0.021	21.16	0.30
III	44	0.070	0.026	21.29	0.32
			This Paper		
I	12	0.124	0.032	20.76	0.18
I–II	11	0.106	0.028	20.88	0.24
II	21	0.116	0.055	21.09	0.38
II–III ..	18	0.138	0.077	21.08	0.31
III	21	0.117	0.052	21.34	0.29
			Total Sample		
I	25	0.091	0.089	20.83	0.24
I–II	22	0.084	0.194	20.98	0.29
II	44	0.089	0.110	21.05	0.32
II–III ..	40	0.096	0.119	21.13	0.30
III	65	0.086	0.083	21.30	0.31

the mean redshift in our sample increases so markedly with richness. The observed change of 0.3 mag from richness 0 to richness 3 over a range in mean redshift from 0.079 to 0.146, however, requires a q_0 in excess of 7 if the effect is entirely cosmological in origin. Alternatively, an uncertainty of 0.5 in q_0 corresponds to an uncertainty of only 7% in the richness correction. There is also a small (richness, Bautz-Morgan)-relation in the sample. The richness 3 clusters contain a disproportionately large number of Bautz-Morgan (BM) type I clusters, while the richness 4 clusters are primarily Bautz-Morgan types II–III and III. If Bautz-Morgan corrections are applied (see following paragraph), the richness corrections for classes 0 to 4 are -0.07, -0.02, $+0.12$, $+0.23$, and $+0.15$ (vs. -0.10, -0.03, $+0.15$, $+0.29$, and $+0.07$ without BM corrections).

Adopting 21.11 for the mean reduced absolute magnitude for brightest cluster galaxies, we arrive at BM corrections of -0.28, -0.13, -0.06, $+0.02$, and $+0.19$ mag for BM classes I through III (vs. -0.37, -0.13, -0.04, $+0.07$, and $+0.19$ for KSW). The larger KSW correction for BM I is likely to be due to their use of a larger aperture. BM I clusters tend to harbor cD galaxies, and their large envelopes would explain their brightening relative to normal ellipticals as one moved to larger apertures. The Bautz-Morgan classes are distributed fairly homogeneously with distance, as indicated in Table 9, so the conclusions about the BM correction are essentially independent of the cosmological model.

Although both cluster richness and Bautz-Morgan class have definite relations with the luminosity of brightest cluster galaxies, removing their effects does not greatly reduce the cosmic scatter. The clusters of HGT and this paper have an uncorrected dispersion of 0.34 mag. Application of the deduced richness and Bautz-Morgan corrections reduce this value to 0.32 and 0.30 mag, respectively, while the dispersion becomes 0.29 mag if both effects are corrected for. Hoessel (1980) found that both these corrections are subsumed in a structural correction which can be calculated from surface photometry of the galaxy itself, and which arises in a natural way from dynamical evolution. We will investigate this "α-correction" further in the second paper in this series.

The Hubble diagram (apparent magnitude vs. redshift), while quite illustrative of some effects, leaves something to be desired when one wishes to emphasize the geometric effects of various world models. We chose to plot the reduced absolute magnitude against a redshift-related quantity. The motivation for this choice is easy to understand. The calculated absolute magnitudes assume a given world model; if we have selected the correct one and brightest cluster galaxies are standard candles, the points will lie on a horizontal line. The reduced absolute magnitudes described in this paper will be the ordinate. The abscissa is

$$x = \log\left\{\frac{2\left[1+z-(1+z)^{1/2}\right]}{z}\right\} = \log\left[\frac{Z_{1/2}(z)}{Z_1(z)}\right].$$

The advantages of this selection are apparent in Figure

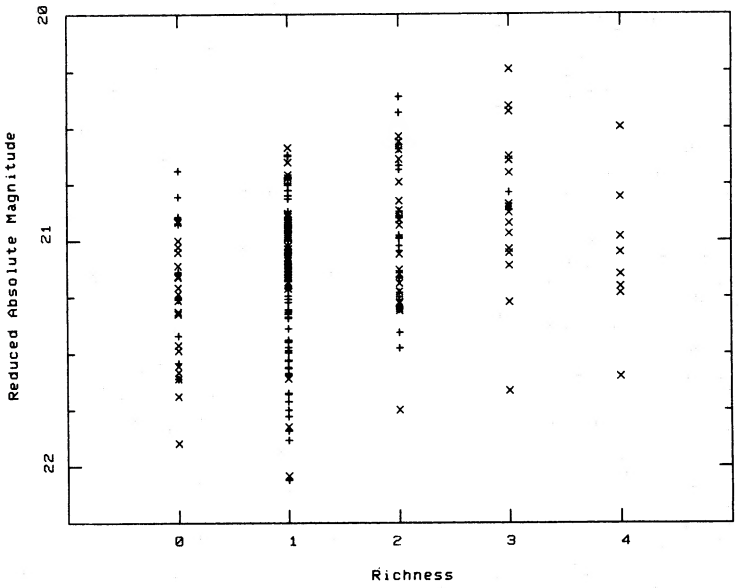

FIG. 7.—The relation between reduced absolute magnitude of brightest cluster galaxies and Abell richness class for HGT (+) and this paper (×). Except for the richness 4 clusters, a correction of ~ 0.1 mag per class represents the data reasonably well.

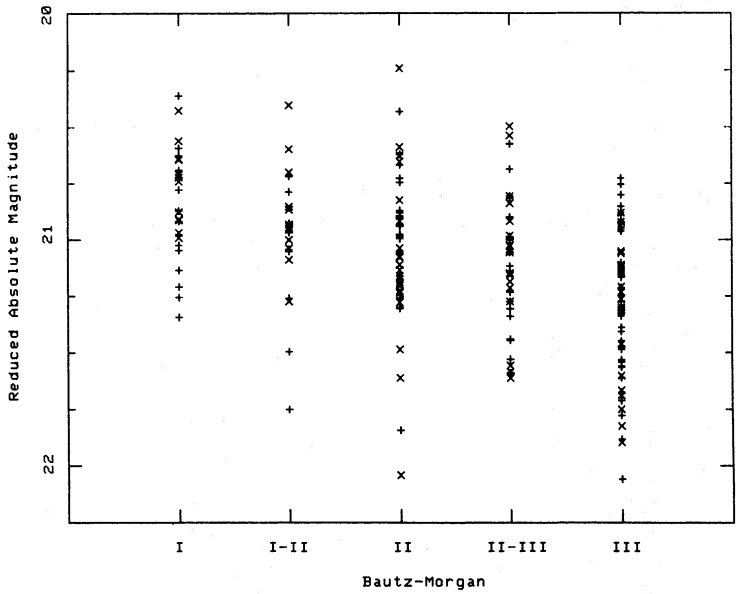

FIG. 8.—Same as Fig. 7 but using Bautz-Morgan class as the abscissa. As the brightest galaxy becomes more dominant, it becomes absolutely brighter.

9, which displays the behavior of reduced absolute magnitudes as a function of z and q_0. All redshifts are contained in Figure 9; the right-hand side corresponds to $z = \infty$ ($x = \log 2 = 0.301$). Note the remarkable linearity of the models. Both the $q_0 = 0.5$ and $q_0 = 1.0$ models are precisely linear. The intercepts at $z = \infty$ are $-5 \log (2q_0)$ (relative to the $q_0 = 0.5$ line, because $Z_q(\infty) = 1/q_0$). The models with q_0 greater than 0.5 (closed universes) lie above our standard $q_0 = 0.5$ line because too large a luminosity distance has been used to calculate the absolute magnitude; the reverse applies to the open models.

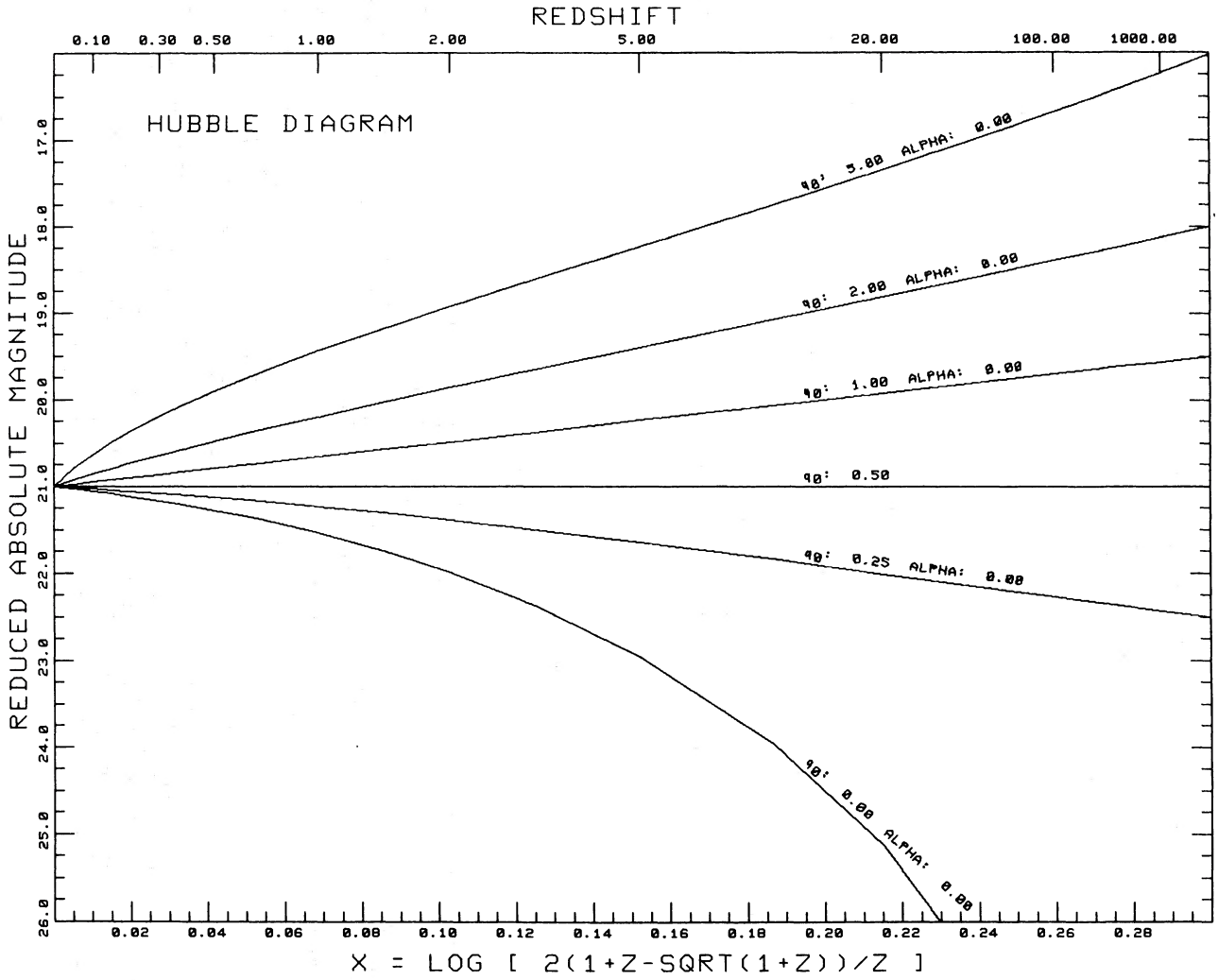

FIG. 9.—The reduced absolute magnitude–redshift relation for various world models. The right-hand edge corresponds to $z = \infty$. The lines represent the behavior of standard candles which have $q_0 = 0.5$ RAMs of 21.0. See text for explanation.

Another feature is the clear presentation of the aperture correction (see GO and Hoessel 1980). If q_0 does not equal 0.5, we are no longer measuring the same metric diameter at different redshifts. Defining

$$\alpha = \left.\frac{d \ln L}{d \ln r}\right|_{r=r_0},$$

GO showed that the sensitivity to q_0 is reduced by the factor $(1 - \alpha/2)$. This appears naturally in our Hubble diagram, for the deviation from the horizontal ($q_0 = 0.5$) line is

$$\mathrm{RAM}_{q_0}(z) - \mathrm{RAM}_{1/2}(z) = (5 - 2.5\alpha) \log \left[\frac{Z_{1/2}(z)}{Z_{q_0}(z)}\right]$$

or

$$(5 - 2.5\alpha)(1 - 2q_0)x \quad \text{for small } x.$$

The rapidity with which the various curves deviate from the $q_0 = 0.5$ line is linear in α, as the above expression shows. If galaxies were point sources ($\alpha = 0$), there is no aperture correction. The sensitivity of the test vanishes for $\alpha = 2$ (constant surface brightness) since there is no cosmological information in surface brightness. We shall show in the following paper in the series that the mean α for our sample is about 0.7, a bit larger than that found by Hoessel (1980) but the same as that used by GO; the aperture correction thus reduces the sensitivity to q_0 by roughly 35%.

In Figure 10 we have plotted the galaxies of HGT, GO, and the richness sample (Tables 5, 6, and 1) on this modified Hubble diagram. Also shown are some world models with $\alpha = 0.7$ and $\langle \mathrm{RAM} \rangle$ of 21.14 from the

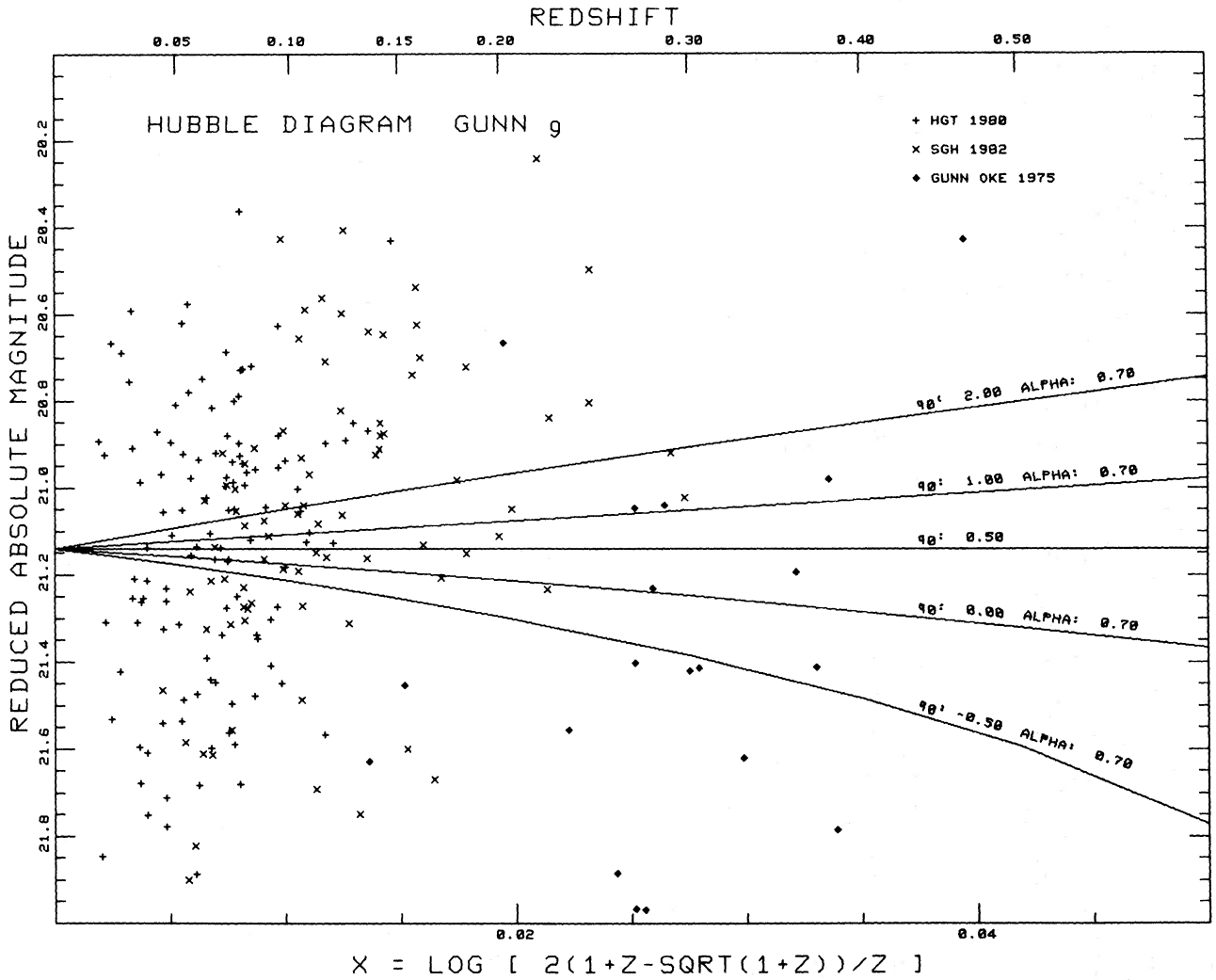

FIG. 10.—Hubble diagram for the galaxies of HGT (+), the richness sample (×), and GO (◇). Some world models with appropriate aperture corrections (α) have been drawn in. The reduced absolute magnitudes are from Tables 5, 1, and 6, respectively.

nearby complete sample of HGT. The $q_0 = -0.5$ model is unphysical, and was obtained simply by evaluating the analytic expression for $Z_{q_0}(z)$ for that value of q_0. The first-order cosmological effects are dependent on q_0 alone, and the curve shown should be accurate for small redshifts.

It is clear that one can say little of cosmological interest on the basis of data shown; nor was that the object of acquiring data on this sample. The low-redshift end of the Hubble diagram is now, however, pinned down about as well as is possible. The present sample could be enlarged about a factor of 3 without exhausting the Abell catalog within our selection criteria. Based on the good statistics presently in hand, we do not believe such an enlargement would reveal any new effects of great cosmological significance. The next step is clearly to obtain similar observations on a carefully selected sample of clusters at high redshift.

VI. SUMMARY

1. Seventy-five new redshifts for Abell clusters have been measured; the redshifts range from 0.04 to 0.30. Redshifts for all clusters in the LVDB catalog with richness greater than 3 and $|b| > 30°$ have now been determined.

2. A four-filter (*griz*) photometric system is described which is well suited for cosmological investigations using ground-based CCDs. The system has a spectral coverage from 4500 to 9500 Å. Corrections for galactic extinction are determined from the intervening H I column density. Photon based (instead of energy based) *k*-corrections have been calculated for the *griz* system. The rest-frame *g* magnitude ($\lambda = 5242$ Å) has been adopted as the standard measurement for brightest cluster galaxies; the filters allow two-color observations to bracket the redshifted *g* filter for redshifts up to 0.74.

3. The standard distance for calculating absolute magnitudes of brightest cluster galaxies in this paper is one Hubble radius (instead of the standard 10 pc). This procedure removes the dependence of the absolute luminosity on H_0. In the $H_0 = 60$, $q_0 = 0.5$ universe, $R_h = 5000$ Mpc, $z_{R_h} = 0.866$, and the distance modulus is 43.39 mag. The reduced absolute magnitude in this paper refers to the k-corrected g magnitude a galaxy would have if placed at a luminosity distance of 1 Hubble radius.

4. Photometry of 84 brightest cluster galaxies (the richness sample) in the g and r passbands using a CCD detector is presented. Brightest cluster galaxies are defined as the region of maximum light enclosed within an aperture with a metric radius of 16 kpc. The measurements have all been corrected for seeing effects (maximum seeing correction ~ 0.025 mag). The rest frame $(g - r)$ colors of brightest cluster galaxies have a dispersion of only 0.04 mag. There has been no detectable color evolution in giant ellipticals since redshifts of 0.25.

5. The galaxies in the richness sample as well as 135 previous measurements of brightest cluster galaxies have been placed on the reduced absolute magnitude system. The dispersion in the aperture magnitudes is 0.34 mag.

6. Brightest cluster galaxies brighten by 0.1 mag per richness class for richness classes 0 to 3. Richness 4 galaxies, however, are fainter than the richness 3 ones by 0.2 mag.

7. The results of this paper confirm the systematic trend of luminosity with Bautz-Morgan class (0.12 mag per class) found in other studies. The BM I galaxies are on average 0.3 mag brighter than the average brightest cluster galaxy.

8. Application of richness and Bautz-Morgan corrections reduces the dispersion in the luminosity of brightest cluster galaxies to 0.29 mag.

9. Nearly 200 brightest cluster galaxies with redshifts less than 0.3 have been placed on a uniform photometric system; thus the mean luminosity of giant ellipticals at the present epoch is quite well known.

We are indebted to Peter Young for aid in acquiring some of the data and for many timely suggestions, and Maarten Schmidt for several photometric observations. We also thank Jerry Kristian for several useful comments. Jim Westphal, Rich Lucinio, Barbara Zimmerman, and Robert Deverill provided much of the hardware and software that made this project feasible. Juan Carrasco, Skip Staples, and Tom Murphy are thanked for their excellent assistance at the telescopes. Ed Danielson and Dave Jewitt provided some of the filter tracings. This project would not have been possible without the support of NASA through the Space Telescope Wide Field/Planetary Camera Project. This work was partially supported by NSF grant AST 80-15346.

REFERENCES

Abell, G. O. 1958, *Ap. J. Suppl.*, **3**, 211.
Bautz, L. P., and Morgan, W. W. 1970, *Ap. J.* (*Letters*), **162**, L149.
Burstein, D., and Heiles, C. 1978, *Ap. J.*, **225**, 40.
Dixon, R. S. 1970, *Ap. J. Suppl.*, **20**, 1.
Gunn, J. E., Hoessel, J. G., and Oke, J. B. 1983, in preparation.
Gunn, J. E., and Oke, J. B. 1975, *Ap. J.*, **195**, 255 (GO).
Gunn, J. E., and Tinsley, B. M. 1976, *Ap. J.*, **210**, 1.
Gunn, J. E., and Westphal, J. A. 1981, *Proc. SPIE*, **290**, 16.
Hausman, M. A., and Ostriker, J. P. 1978, *Ap. J.*, **224**, 320.
Heiles, C. 1975, *Astr. Ap. Suppl.*, **20**, 37.
Hoessel, J. G. 1980, *Ap. J.*, **241**, 493.
Hoessel, J. G., Gunn, J. E., and Thuan, T. X. 1980, *Ap. J.*, **241**, 486 (HGT).
Humason, M. L., Mayall, N. U., and Sandage, A. R. 1956, *A.J.*, **61**, 97 (HMS).
Johnson, H. L. 1968, in *Nebulae and Interstellar Matter*, ed. B. Middlehurst and L. Aller (Chicago and London: University of Chicago Press), p. 167.
Kristian, J. A., Sandage, A., and Westphal, J. A. 1978, *Ap. J.*, **221**, 383 (KSW).
Leir, A. A., and van den Bergh, S. 1977, *Ap. J. Suppl.*, **34**, 381 (LVDB).
Oemler, A. 1974, *Ap. J.*, **194**, 1.
Oke, J. B., and Schild, R. E. 1971, *Ap. J.*, **161**, 1015.
Ostriker, J. P., and Tremaine, S. D. 1975, *Ap. J.* (*Letters*), **202**, L113.
Sandage, A. 1961, *Ap. J.*, **133**, 335.
_____. 1973, *Ap. J.*, **183**, 711.
Sandage, A., Kristian, J. A., and Westphal, J. A. 1976, *Ap. J.*, **205**, 688 (SKW).
Sargent, W. L. W. 1973, *Pub. A.S.P.*, **85**, 281.
Sargent, W. L. W., Schechter, P. L., Boksenberg, A., and Shortridge, K. 1977, *Ap. J.*, **212**, 326.
Schechter, P. L., and Gunn, J. E. 1979, *Ap. J.*, **229**, 472.
Schmidt, M. 1965, *Ap. J.*, **141**, 1.
Schneider, D. P. 1983, preprint.
Schneider, D. P., and Gunn, J. E. 1982, *Ap. J.*, **263**, in press.
Schneider, D. P., Gunn, J. E., and Hoessel, J. G. 1983, preprint (Paper II).
Stark, A., and Heiles, C. 1981, preprint.
Thuan, T. X., and Gunn, J. E. 1976, *Pub. A.S.P.*, **88**, 543 (TG).
Tinsley, B. M., and Gunn, J. E. 1976, *Ap. J.*, **206**, 525.
Wade, R. A., Hoessel, J. G., Elias, J. H., and Huchra, J. P. 1979, *Pub. A.S.P.*, **91**, 35.
Weinberg, S. 1972, *Gravitation and Cosmology* (New York: Wiley).
Whitford, A. E. 1971, *Ap. J.*, **169**, 215.
Young, P., Schneider, D. P., and Shectman, S. A. 1981, *Ap. J.*, **244**, 259.

JAMES E. GUNN: Peyton Hall, Princeton University Observatory, Princeton, NJ 08540

JOHN G. HOESSEL: Space Telescope Science Institute, Homewood Campus, Baltimore, MD 21218

DONALD P. SCHNEIDER: 105-24 Robinson Laboratory, California Institute of Technology, Pasadena, CA 91125